Antitumor Agents

Deutsche Ausgabe: DOI: 10.1002/ange.201509432
Internationale Ausgabe: DOI: 10.1002/anie.201509432

Structurally Defined αMHC-II Nanobody–Drug Conjugates: A Therapeutic and Imaging System for B-Cell Lymphoma

*Tao Fang, Joao N. Duarte, Jingjing Ling, Zeyang Li, Jonathan S. Guzman, and Hidde L. Ploegh**

Abstract: *Antibody–drug conjugates (ADCs) of defined structure hold great promise for cancer therapies, but further advances are constrained by the complex structures of full-sized antibodies. Camelid-derived single-domain antibody fragments (VHHs or nanobodies) offer a possible solution to this challenge by providing expedited target screening and validation through switching between imaging and therapeutic activities. We used a nanobody (VHH7) specific for murine MHC-II and rendered "sortase-ready" for the introduction of oligoglycine-modified cytotoxic payloads or NIR fluorophores. The VHH7 conjugates outcompeted commercial monoclonal antibodies (mAbs) for internalization and exhibited high specificity and cytotoxicity against A20 murine B-cell lymphoma. Non-invasive NIR imaging with a VHH7–fluorophore conjugate showed rapid tumor targeting on both localized and metastatic lymphoma models. Subsequent treatment with the nanobody–drug conjugate efficiently controlled tumor growth and metastasis without obvious systemic toxicity.*

B-cell lymphoma is the most common type of non-Hodgkin's lymphoma (NHL). The American Cancer Society estimates that in 2015, approximately 70000 new cases of NHL will be diagnosed in the United States, with mortality around 20000 patients. Antibodies against a variety of cellular receptors or antigens on B cells such as CD20,[1] surface immunoglobulins,[2] Class II major histocompatibility complex antigens (MHC-II),[3] CD80/CD86,[4] and CD40[5] have shown efficacy in treating B-cell malignancies. Therapeutic mAbs or ADCs such as Rituximab or Brentuximab, which target CD20 and CD30 respectively represent significant advances in the management of B-cell malignancies.

Without exception, ADCs in the clinic so far rely on full-sized mAbs and on a rather limited range of conjugation methods, at times resulting in heterogeneous mixtures.[6] Accurate prediction of the drug:antibody ratio (DAR), which crucial to the pharmaceutical properties of ADCs and the translation of the manufacturing process from one antibody to another,[7] requires sophisticated mass spectroscopic methods and time-consuming empirical optimizations.[8] Recent efforts in making homogeneous ADCs[9] have involved direct genetic approaches to install reactive cysteine residues,[10] unnatural amino acids,[11,12] and formylglycine-generating enzyme[13] or sortase[14] recognition motifs, as well as indirect glyco-[15,16] or metabolic[17] engineering of the conserved N-glycan of the IgG Fc domain. The structural complexity and post-translational modifications of mAbs complicate the straightforward expression and preparation of functionalized mAbs. To simplify mAbs while retaining essential functions, antibody fragments (scFv and Fab) and their engineered variants (diabodies, triabodies, minibodies) are the smaller formats of choice.[18] Similar conjugation methods are generally transferable to antibody fragments. Their conjugates with radioactive tracers,[19,20] nanomaterials,[21,22] gene products,[23] immunomodulators,[24] cytotoxic reagents,[25,26] or a combination[27] have demonstrated great potential in therapeutic and diagnostic applications.

Following the discovery of unique heavy-chain-only antibodies in the family of *Camelidae*,[28] it was shown that their variable domains (VHHs), the smallest naturally derived antigen-binding fragment (ca. 15 kDa), retain antigen-binding capacity when expressed recombinantly. The small size of VHHs greatly benefits rapid circulatory clearance and reduces background in an non-invasive imaging setting.[19,29] Their single-domain nature allows convenient phagemid-based screening. The inherent absence of a hydrophobic surface that is usually present between V_H and V_L improves VHH solubility, providing high yield (50 mg L^{-1}) in an *E. coli* expression system. No major framework rearrangements of VHHs have been observed, while the CDR3 domain is primarily involved in antigen binding and protrudes from the remaining binding surface, with the C terminus extending in the opposite direction.[30] This justifies the installation of a C-terminal pentapeptide sortase recognition motif (LPXTG), which in turn provides nearly limitless possibilities for site-specific modifications without compromising the binding properties of the modified VHHs.[31–33] Collectively, nanobody–drug conjugates are desirable targets for the development the next generation of ADCs.[34]

We identified a VHH (VHH7) that binds murine class II major histocompatibility complex (MHC-II) molecules with low nanomolar affinity. MHC-II is expressed on professional antigen-presenting cells such as dendritic cells, B-cells, and macrophages. Compared to other B-cell markers like CD20, MHC-II is highly expressed on the B-cell surface (8×10^4/cell for MHC-II vs. 9×10^3/cell for CD20)[35,36] and can be upregulated after antibody or immunostimulant treatment with rituximab, CpG,[37] or IFN-γ.[38] Single-agent therapy with

[*] Dr. T. Fang, Dr. J. N. Duarte, J. Ling, Z. Li, J. S. Guzman, Prof. Dr. H. L. Ploegh
Whitehead Institute for Biomedical Research
9 Cambridge Center, Cambridge, MA 02142 (USA)
E-mail: ploegh@wi.mit.edu
J. S. Guzman, Prof. Dr. H. L. Ploegh
Department of Biology, Massachusetts Institute of Technology
Cambridge, MA 02139 (USA)
J. Ling, Z. Li
Department of Chemistry, Massachusetts Institute of Technology
Cambridge, MA 02139 (USA)

Supporting information for this article is available on the WWW under http://dx.doi.org/10.1002/anie.201509432.

 © 2016 Wiley-VCH Verlag GmbH & Co. KGaA, Weinheim

two courses of Rituximab lead to the outgrowth of CD20-negative variants in NHL patients, thus indicating a need for complimentary targets.[39]

We report herein the preparation of a structurally defined nanobody–drug conjugate (VHH7-DM1) by using sortase-mediated site-specific protein engineering, as well as its pharmacokinetics and in vivo targeting as corroborated by non-invasive optical imaging. The therapeutic benefit of this conjugate was shown through the treatment of both localized and disseminated murine B-cell lymphoma, using the A20 cell line as a model.

To prepare a structurally defined VHH7–drug conjugate, we chose the thiol-containing Maytansine derivative Mertansine (DM1) as our cytotoxic payload. DM1 is a potent inhibitor of microtubule polymerization that has no useful therapeutic window when used as a single agent, but has been used to create ADCs.[40] In studies of Trastuzumab emtansine (Kadcyla), it was shown that conjugation of DM1 to mAbs through a non-cleavable succinimidyl 4-(*N*-maleimidomethyl)cyclohexane-1-carboxylate (SMCC) linker, followed by proteolytic degradation of this construct in endosomes/lysosomes, gave favorable clinical results in a phase III trial compared to the use of a cleavable disulfide linker.[41] Accordingly, we explored the sequential thiol-Michael ligation of a bis(maleimido)ethane (BMOE) linker[42] with the free mercapto group of hydrophilic peptide **1** and DM1 (Figure 1a). When using 5 equivalents of BMOE, peptide **1** is labeled monovalently and quantitatively after 16 h at room temperature in DMF. Excess BMOE was precipitated by the addition of water and the reaction mixture was purified by RP-HPLC, lyophilized, and then converted into **2** after reaction with 2 equivalents of DM1 to give 80% conversion after 16 h, based on the integration of the HPLC trace. The sortase reaction between VHH7 and **2** was carried out by following established methods[43,44] in which unreacted VHH7 and sortase are removed by incubation with Ni-NTA agarose beads, leaving product **3** and excess nucleophile **2**, which were easily separated by size-exclusion chromatography (SEC) to obtain the desired product **3**. The identity of the conjugate was confirmed by LC–MS (Figure 1b) and when analyzed by SDS-PAGE, the product appeared as a single band (Figure 1c).

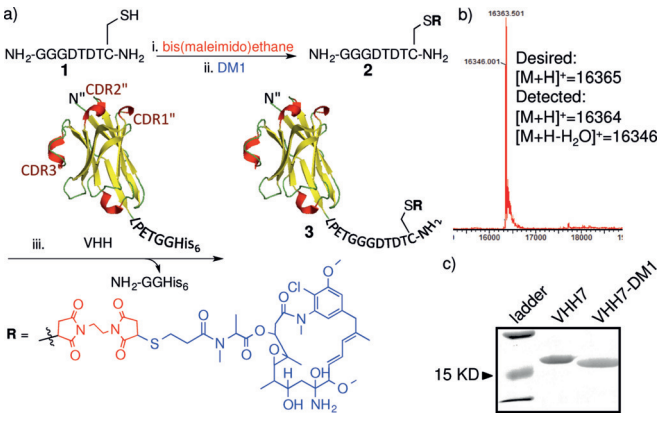

Figure 1. Synthesis and characterization of a structurally defined VHH7–DM1 conjugate. a) Preparation of the VHH7–DM1 conjugate. Conditions: i) DMF, RT 2 h; ii) DMF/PBS = 4:1 (v/v), 18 °C, 16 h; iii) Srt A (pentamutant), 10 mM $CaCl_2$, 50 mM Tris, pH 7.4, 12 °C, 2–4 h; b) LC–MS analysis of VHH7–DM1; c) SDS-PAGE analysis of the VHH7–DM1 conjugate (15% gel, InstantBlue, faster mobility of VHH7–DM1 was due to the cyclic structure of DM1, LC–MS profile in Figure S1c). DMF = dimethylformamide, PBS = phosphate-buffered saline, Srt A = sortase A.

We also modified VHHs with the NIR dye Alexa Fluor 647 (AF647) through sortagging. Binding of VHH7 to MHC-II-positive A20 cells was measured at various concentrations of VHH7–AF647 and assessed by flow cytometry, and the results show a half maximal binding concentration (EC_{50}) of 2.1 nM (Figure 2a). Kinetics of VHH7 internalization were

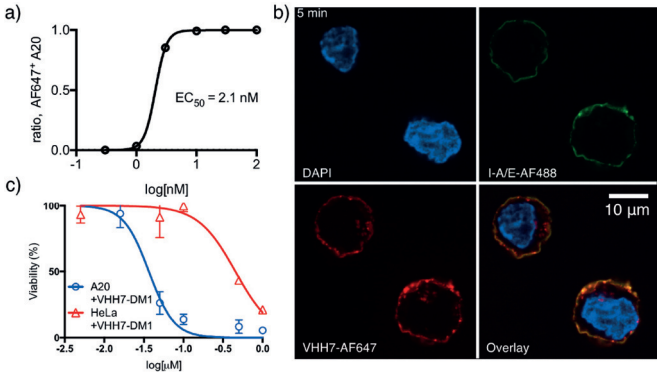

Figure 2. In vitro characterization of the VHH7 conjugates. a) Determination of the half maximal effective binding concentration (EC_{50}) of VHH7–AF647 with murine lymphoma A20 cells. 5×10^5 cells were incubated with increasing concentrations of VHH7–AF647 at 4 °C for 1 h, then washed three times and analyzed by flow cytometry. b) Internalization of commercial antibody anti-I-A/E–AF488 (M5/114.15.2) and VHH7–AF647. Equal molar amounts of VHH–AF647 and anti-I-A/E–AF488 were premixed and added to cells in a poly-L-lysine-coated imaging chamber at a final concentration of 50 nM. After 5 min, the cells were washed with ice-cold PBS, then fixed and mounted for confocal microscopy. c) In vitro cytoxocity of the VHH7–DM1 conjugate againsy MHC-II-positive (A20) and MHC-II–negative (Hela) cell lines ($n = 3$, error bars = mean ± SD).

determined by incubating A20 cells with VHH7–AF647, a genetic dimer with a tandem N-to-C arrangement of two VHH7 units with a single C-terminal AF647, a commercial anti-I-A/E antibody anti-I-A/E IgGκ–AF488, or an anti-human integrin VHH (2B7) as a negative control, followed by surface staining with anti-IgG–AF591 and analysis by confocal microscopy (Figure S3; I-A/E = MHC Class II alloantigens I-A, I-E, IgG = immunoglobulin G). Monovalent VHH7–AF647 was internalized within 1 h, while internalization of the commercial anti-I-A/E reagent was observed only after overnight incubation. We next tested the internalization of the VHH7 genetic dimer. A similar rate of internalization was observed for the dimer when applied at the same concentration. We performed a competition study by co-incubating A20 cells with VHH7–AF647 and anti-I-A/E IgGκ–AF488, and observed that VHH7 was internalized rapidly and appeared in vesicular structures within 5 min, leaving the commercial anti-I-A/E reagent visible as a rim

 © 2016 Wiley-VCH Verlag GmbH & Co. KGaA, Weinheim

stain (Figure 2b). The rapid internalization of VHH7 upon binding to MHC-II suggests potential for use in targeted drug delivery. In contrast, anti-CD20 is not internalized as rapidly, thus making it a better mediator of antibody-dependent cell-mediated cytotoxicity (ADCC).[45] An anti-EGFR nanobody also showed slow internalization.[46] The choice of target as it relates to its internalization is thus an important parameter in the design of VHH–drug conjugates.

We studied the in vitro cytotoxicity of the VHH7–DM1 conjugate against murine lymphoma A20 cells, as well as MHC-II-negative cell lines such as HeLa and HEK293 (Figure 2c and Figure S2). Cells (4×10^4 per well in a 96 well plate) were exposed to VHH7–DM1 or to unconjugated DM1 at increasing concentrations. The VHH7–DM1 fusion effectively killed A20 cells with a half maximal inhibitory concentration (IC_{50}) of 36 nM, whereas the HeLa and HEK293 cells required around 500 nM to see the same effect (Figure S2), thus demonstrating the selective action of the VHH7–DM1 fusion. The unconjugated drug shows similar cytotoxicity for all three cell lines.

We confirmed systemic targeting of A20 lymphoma in both localized and metastatic models by non-invasive optical imaging. We detected the subcutaneous tumor after intravenous (iv) injection of VHH7–AF647 as monitored by IVIS (Figure 3a,b). Injection of an irrelevant control nanobody–AF647 conjugate (Enh–AF647) into an A20-bearing mouse, or injection of VHH–AF647 into a MHC-II knockout (KO) mouse resulted in rapid clearance without signs of non-specific binding at the tumor site. The average radiant efficiency of the tumor and the S/N ratios at different time points (Figure S6) suggest that in vivo targeting reached a maximum at 30 min and persisted over the next 96 h. The signal from the kidney reached its maximum within 5 h and then progressively decreased, which is consistent with the kidneys being the major clearance pathway for VHHs.[47] Targeting at the cellular level was also confirmed when tumors were removed 2 h post injection (p.i.) of VHH7–AF647 or Enh–AF647, frozen, sectioned, and mounted for confocal microscopy (Figure S4). Vesicular structures were observed for samples from VHH7–AF647-injected mice, while no signal was detected for Enh–AF647.

The lungs, liver, spleen, and lymph nodes are possible sites of invasion in the case of disseminated lymphoma. We observed strong signals from the lungs and liver by NIR imaging (Figure 3c,d), whereas signals from healthy Balb/c mice mainly emanated from the GI tract and bladder. To confirm targeting of VHH7 to metastatic foci, both healthy and tumor-bearing mice were injected with 40 μg VHH7–AF647 and dissected, followed by comparison of fluorescence signals from the lungs, liver, and spleen (Figure 3e). The presence of lymphoma in these organs was first confirmed cytologically. Metastasic foci were found in the liver, with splenomegaly as a consequence of tumor infiltration. NIR imaging was consistent with the cytological observations: all tumor-bearing organs showed strong fluorescence signals. The fluorescence signal persists even after 24 h owing to retention of VHH7 at the tumor site, with delayed clearance compared to healthy mice (Figure 3f,g). A meaningful comparison of the biodistribution of VHH7 and full-sized α-I-A/E would require a full-sized Ab of the identical specificity and labelled to the same intensity, a preparation that we currently lack. VHH7–AF647 is monovalently labelled, while the full-sized α-I-A/E–AF647 has 8–10 fluorophores per molecule. When VHH7 and full-sized α-I-A/E were injected at the same fluorescent dose, a stronger signal was seen for VHH7 at the tumor site (Figure 3h). Injection of similar molar quantities of VHH7 and full-sized α-I-A/E showed increased staining of VHH7 for spleen and inguinal lymph nodes compared to α-I-A/E (Figure S8).

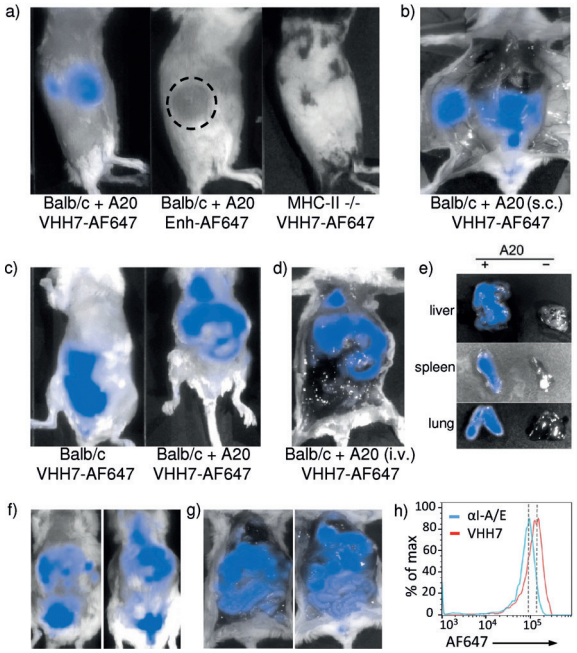

Figure 3. Non-invasive NIR imaging of A20 lymphoma by using the VHH7–AF647 conjugate. (color scale: full range, minimum to maximum). a) Balb/c mice with subcutaneous A20 lymphoma (left, middle) and MHC-II KO mouse (right) were injected with 40 μg VHH7–AF647 or control Enh–AF647 conjugate as shown, then imaged by using an in vivo imaging system (IVIS). Pictures show 5 h p.i. (black dashed circle highlights tumor burden). b) A mouse with subcutaneous A20 lymphoma was dissected 16 h p.i. of VHH7–AF647 to show clear tumor targeting. c) Healthy (left) and intravenously A20-inoculated (right, 4 weeks p.i.) Balb/c mice were imaged 5 h p.i. of VHH7–AF647. d) A mouse with metastatic A20 lymphoma was dissected 5 h p.i. of VHH7–AF647 to show clear tumor targeting in lung, liver, and spleen. e) Organs from metastatic and healthy mice (from (c)) were imaged in the same view. f) Two Balb/c mice with disseminated A20 lymphoma (4 weeks after inoculation) were imaged 24 h p.i. of VHH7–AF647. g) Mice from (f) were dissected to show targeting at tumor sites. h) Comparable doses (6400 RFU) of fluorescently labeled VHH7–AF647 and α-I-A/E–AF647 were injected into mice bearing subcutaneous tumors. RFU = relative fluorescence units. The tumors were removed and analyzed by flow cytometry. Shift in mean fluorescence intensity: 92K (α-I-A/E) to 135K (VHH7).

Finally, the VHH7–DM1 conjugate was subjected to tests in vivo to treat the highly invasive A20 lymphoma, which is known to target the spleen, liver, and lymph nodes. The A20 tumors are radioresistant at myeloablative doses of radiation and only poorly immunogenic. Neither radiation nor vaccine therapy affords protection.[48] We first engrafted A20 cells subcutaneously to monitor the progression of a single tumor

© 2016 Wiley-VCH Verlag GmbH & Co. KGaA, Weinheim

at a known site. The tumors were allowed to grow until the average volume reached 150 mm^3. Starting at day ten p.i., a total of five doses of VHH7–DM1 at 125 μg/injection (5 $mg\,kg^{-1}$) were administered every other day, with daily monitoring of tumor size (Figure 4a). Final sizes of tumors in the VHH7–DM1-treated group remained significantly smaller than those in the PBS-treated control [mean: 1479 mm^3 (controls) vs. 480 mm^3 (VHH7–DM1 treated), $p = 0.012$, $n = 3$]. Mice treated with VHH7 alone were no different from the controls ($p = 0.99$). We next explored the disseminated A20 model. After iv injection of A20 cells, treatment started the next day at 125 μg/injection (5 $mg\,kg^{-1}$) every other day for a total of four injections. Mice were sacrificed on day 27 when metastatic foci in the livers of the control group became palpable. We enumerated the liver foci for untreated and VHH7/Enh–DM1-treated groups (Figure 4b). The efficacy of VHH7–DM1 in limiting metastasic spread is encouraging, in that no more than three small foci ($\Phi < 3$ mm) were found for the treated group. In untreated animals and in the Enh–DM1-treated group, massive liver metastases [liver weight = 4.8 ± 0.87 g (mean ± SD), $n = 5$, normal weight ≈ 1.4 g] were observed, with up to 30 foci. Survival was monitored in a parallel experiment (Figure S7). After four injections, VHH7–DM1-treated mice showed an increased median survival of 44 days, compared to 29 days for animals treated with Enh–DM1. No nephrotoxicity was observed after six injections, as inferred from creatinine levels [0.27 ± 0.06 $mg\,mL^{-1}$ (mean ± SD), $n = 3$, normal range 0–1 $mg\,mL^{-1}$]. Injection of healthy mice with two doses of VHH7–DM1, followed by flow cytometry analysis of splenocytes five days later did not show significant differences in the MHC-II$^+$ populations [CD19$^+$ (B-cells): 52.1% vs. 51.3%; CD11b$^+$CD11c$^-$ (macrophages): 1.7% v.s. 1.6%; CD11b$^+$CD11c$^+$ (dendritic cells): 0.4% vs. 0.3%; control vs. injection; average of two].

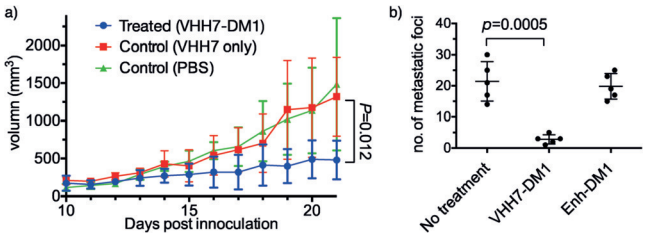

Figure 4. In vivo efficiency of the VHH7–DM1 conjugate in treating A20 lymphoma. a) The VHH7–DM1 conjugate inhibited tumor growth in a localized model. Nine Balb/c mice were subcutaneously inoculated with 2.5×10^6 A20 cells then randomized into three groups at day ten when tumor burdens became measurable by caliper. Starting at day ten, samples were given iv at a dose of 125 μg/mice (5 $mg\,kg^{-1}$ for 25 g mice) and followed every other day for a total of five injections. Tumor volume (V) was used to evaluate tumor size by using a modified ellipsoid formula: $V = (\text{width})^2 \text{length}/2$ (error bars: mean ± SD, $n = 3$). Experiment end point was defined as when the largest single-tumor size exceeded 2000 mm^3. b) VHH7–DM1 protected mice from tumor metastasis in a disseminated model. Fifteen Balb/c mice were subcutaneously inoculated with 1.5×10^6 A20 cells and then randomized into three groups. Injection started at day two, with a dose of 125 μg/mice and followed every other day for a total of four injections. Mice were sacrificed on day 27, and the number of metastatic foci on liver was counted (error bars: mean ± SD, $n = 5$).

In summary, we generated a homogeneous anti-MHC-II nanobody–drug conjugate (VHH7–DM1) through sortase-mediated protein conjugation. The conjugate was characterized in vivo and in vitro and was efficient in treating an aggressive murine B-cell lymphoma. The favorable pharmacokinetics of the VHH conjugates means that they outcompete the commercial mAb for internalization and clearance, thereby providing reduced systemic cytotoxicity and convenient non-invasive imaging.

Acknowledgements

This research was supported by NIH (R01AI087879) and NIH DP1 GM106409. We thank the Whitehead Institute flow cytometry facility, W. M. Keck biological imaging facility (N. Watson and W. Salmon) and Preclinical Imaging Core of the Koch Institute (S. Malstrom) for instrument usage. J.N.D. is a Calouste Gulbenkian scholar, funded by the Calouste Gulbenkian Foundation, Champalimaud Foundation, Portuguese Science and Technology Foundation and Portuguese Ministry of Health.

Keywords: sortase · antibody–drug conjugates · antitumor agents · imaging agents · nanobodies

How to cite: *Angew. Chem. Int. Ed.* **2016**, *55*, 2416–2420
Angew. Chem. **2016**, *128*, 2462–2466

[1] D. Shan, J. A. Ledbetter, O. W. Press, *Blood* **1998**, *91*, 1644–1652.
[2] M. Mayumi, S. Sumimoto, S. Kanazashi, D. Hata, K. Yamaoka, Y. Higaki, T. Ishigami, K. M. Kim, T. Heike, K. Katamura, *J. Allergy Clin. Immunol.* **1996**, *98*, S238–247.
[3] M. Dechant, J. Bruenke, T. Valerius, *Semin. Oncol.* **2003**, *30*, 465–475.
[4] Z.-Z. Yang, A. J. Novak, S. C. Ziesmer, T. E. Witzig, S. M. Ansell, *Cancer Res.* **2009**, *69*, 5522–5530.
[5] M. von Bergwelt-Baildon, *Ann. Oncol.* **2004**, *15*, 853–857.
[6] A. Mullard, *Nat. Rev. Drug Discovery* **2013**, *12*, 329–332.
[7] B.-Q. Shen, K. Xu, L. Liu, H. Raab, S. Bhakta, M. Kenrick, K. L. Parsons-Reponte, J. Tien, S.-F. Yu, E. Mai et al., *Nat. Biotechnol.* **2012**, *30*, 184–189.
[8] V. S. Goldmacher, G. Amphlett, L. Wang, A. C. Lazar, *Mol. Pharm.* **2015**, *14*, 1605–1613.
[9] P. Agarwal, C. R. Bertozzi, *Bioconjugate Chem.* **2015**, *26*, 176–192.
[10] J. R. Junutula, H. Raab, S. Clark, S. Bhakta, D. D. Leipold, S. Weir, Y. Chen, M. Simpson, S. P. Tsai, M. S. Dennis et al., *Nat. Biotechnol.* **2008**, *26*, 925–932.
[11] S. A. Kularatne, V. Deshmukh, J. Ma, V. Tardif, R. K. V. Lim, H. M. Pugh, Y. Sun, A. Manibusan, A. J. Sellers, R. S. Barnett et al., *Angew. Chem. Int. Ed.* **2014**, *53*, 11863–11867; *Angew. Chem.* **2014**, *126*, 12057–12061.
[12] J. Y. Axup, K. M. Bajjuri, M. Ritland, B. M. Hutchins, C. H. Kim, S. A. Kazane, R. Halder, J. S. Forsyth, A. F. Santidrian, K. Stafin et al., *Proc. Natl. Acad. Sci. USA* **2012**, *109*, 16101–16106.
[13] P. Agarwal, J. van der Weijden, E. M. Sletten, D. Rabuka, C. R. Bertozzi, *Proc. Natl. Acad. Sci. USA* **2013**, *110*, 46–51.

 © 2016 Wiley-VCH Verlag GmbH & Co. KGaA, Weinheim

[14] R. R. Beerli, T. Hell, A. S. Merkel, U. Grawunder, *PLoS One* **2015**, *10*, e0131177.
[15] X. Li, T. Fang, G. J. Boons, *Angew. Chem. Int. Ed.* **2014**, *53*, 7179 – 7182; *Angew. Chem.* **2014**, *126*, 7307 – 7310.
[16] E. L. Smith, J. P. Giddens, A. T. Iavarone, K. Godula, L.-X. Wang, C. R. Bertozzi, *Bioconjugate Chem.* **2014**, *25*, 788 – 795.
[17] N. M. Okeley, B. E. Toki, X. Zhang, S. C. Jeffrey, P. J. Burke, S. C. Alley, P. D. Senter, *Bioconjugate Chem.* **2013**, *24*, 1650 – 1655.
[18] P. Holliger, P. J. Hudson, *Nat. Biotechnol.* **2005**, *23*, 1126 – 1136.
[19] A. C. Freise, A. M. Wu, *Mol. Immunol.* **2015**, *67*, 142 – 152.
[20] S. Massa, C. Xavier, J. De Vos, V. Caveliers, T. Lahoutte, S. Muyldermans, N. Devoogdt, *Bioconjugate Chem.* **2014**, *25*, 979 – 988.
[21] G.-Y. Chen, Z. Li, C. S. Theile, N. M. Bardhan, P. V Kumar, J. N. Duarte, T. Maruyama, A. Rashidfarrokh, A. M. Belcher, H. L. Ploegh, *Chem. Eur. J.* **2015**, *21,* 17178 – 17183.
[22] J. Ahn, Y. Miura, N. Yamada, T. Chida, X. Liu, A. Kim, R. Sato, R. Tsumura, Y. Koga, M. Yasunaga et al., *Biomaterials* **2015**, *39*, 23 – 30.
[23] E. Sadeqzadeh, F. Rahbarizadeh, D. Ahmadvand, M. J. Rasaee, L. Parhamifar, S. M. Moghimi, *J. Controlled Release* **2011**, *156*, 89 – 95.
[24] N. Pasche, D. Neri, *Drug Discovery Today* **2012**, *17*, 583 – 590.
[25] Y. Cao, J. W. Marks, Z. Liu, L. H. Cheung, W. N. Hittelman, M. G. Rosenblum, *Oncogene* **2014**, *33*, 429 – 439.
[26] K. M. Kim, C. F. McDonagh, L. Westendorf, L. L. Brown, D. Sussman, T. Feist, R. Lyon, S. C. Alley, N. M. Okeley, X. Zhang et al., *Mol. Cancer Ther.* **2008**, *7*, 2486 – 2497.
[27] T. List, G. Casi, D. Neri, *Mol. Cancer Ther.* **2014**, *13*, 2641 – 2652.
[28] C. Hamers-Casterman, T. Atarhouch, S. Muyldermans, G. Robinson, C. Hammers, E. B. Songa, N. Bendahman, R. Hammers, *Nature* **1993**, *363*, 446 – 448.
[29] M. Rashidian, E. J. Keliher, A. M. Bilate, J. N. Duarte, G. R. Wojtkiewicz, J. T. Jacobsen, J. Cragnolini, L. K. Swee, G. D. Victora, R. Weissleder et al., *Proc. Natl. Acad. Sci. USA* **2015**, *112*, 6146 – 6151.
[30] A. Desmyter, T. R. Transue, M. A. Ghahroudi, M.-H. Dao Thi, F. Poortmans, R. Hamers, S. Muyldermans, L. Wyns, *Nat. Struct. Biol.* **1996**, *3*, 803 – 811.
[31] M. W. Popp, J. M. Antos, G. M. Grotenbreg, E. Spooner, H. L. Ploegh, *Nat. Chem. Biol.* **2007**, *3*, 707 – 708.
[32] Z. Li, C. S. Theile, G.-Y. Chen, A. M. Bilate, J. N. Duarte, A. M. Avalos, T. Fang, R. Barberena, S. Sato, H. L. Ploegh, *Angew. Chem. Int. Ed.* **2015**, *54*, 11706 – 11710; *Angew. Chem.* **2015**, *127*, 11872 – 11876.
[33] M. D. Witte, J. J. Cragnolini, S. K. Dougan, N. C. Yoder, M. W. Popp, H. L. Ploegh, *Proc. Natl. Acad. Sci. USA* **2012**, *109*, 11993 – 11998.
[34] M. Kijanka, B. Dorresteijn, S. Oliveira, P. M. van Bergen en Henegouwen, *Nanomedicine* **2015**, *10*, 161 – 174.
[35] S. Demotz, H. M. Grey, A. Sette, *Science* **1990**, *249*, 1028 – 1030.
[36] L. Ginaldi, M. De Martinis, E. Matutes, N. Farahat, R. Morilla, D. Catovsky, *J. Clin. Pathol.* **1998**, *51*, 364 – 369.
[37] B. Jahrsdörfer, G. Hartmann, E. Racila, W. Jackson, L. Mühlenhoff, G. Meinhardt, S. Endres, B. K. Link, A. M. Krieg, G. J. Weiner, *J. Leukocyte Biol.* **2001**, *69*, 81 – 88.
[38] M. Zhao, F. L. Flynt, M. Hong, H. Chen, C. A. Gilbert, N. T. Briley, S. C. Bolick, K. L. Wright, J. F. Piskurich, *Mol. Immunol.* **2007**, *44*, 2923 – 2932.
[39] T. A. Davis, D. K. Czerwinski, R. Levy, *Clin. Cancer Res.* **1999**, *5*, 611 – 615.
[40] C. Tan in *Antibody-Drug Conjug. SE-2* (Eds.: J. Wang, W.-C. Shen, J. L. Zaro), Springer International Publishing, Heidelberg, **2015**, pp. 11 – 22.
[41] H. K. Erickson, P. U. Park, W. C. Widdison, Y. V. Kovtun, L. M. Garrett, K. Hoffman, R. J. Lutz, V. S. Goldmacher, W. A. Blattler, *Cancer Res.* **2006**, *66*, 4426 – 4433.
[42] The degradation of thiol-Micheal adducts has been reported; however, this process is generally slow when compared to the clearance of VHHs. The improvement in stability is referred to in comparison with disulfide or hydrazone linkers.
[43] C. S. Theile, M. D. Witte, A. E. M. Blom, L. Kundrat, H. L. Ploegh, C. P. Guimaraes, *Nat. Protoc.* **2013**, *8*, 1800 – 1807.
[44] C. P. Guimaraes, M. D. Witte, C. S. Theile, G. Bozkurt, L. Kundrat, A. E. M. Blom, H. L. Ploegh, *Nat. Protoc.* **2013**, *8*, 1787 – 1799.
[45] P. Boross, J. H. W. Leusen, *Am. J. Cancer Res.* **2012**, *2*, 676 – 690.
[46] R. Heukers, P. M. P. van Bergen en Henegouwen, S. Oliveira, *J. Nanomed. Nanotechnol. Biol. Med.* **2014**, *10*, 1441 – 1451.
[47] J. De Vos, N. Devoogdt, T. Lahoutte, S. Muyldermans, *Expert Opin. Biol. Ther.* **2013**, *13*, 1149 – 1160.
[48] M. Graner, A. Raymond, D. Romney, L. He, L. Whitesell, E. Katsanis, *Clin. Cancer Res.* **2000**, *6*, 909 – 915.

Received: October 8, 2015
Revised: December 6, 2015
Published online: January 14, 2016

 © 2016 Wiley-VCH Verlag GmbH & Co. KGaA, Weinheim